International Journal of Remote Sensing, 2015
Vol. 36, No. 8, 2076–2092, http://dx.doi.org/10.1080/01431161.2015.1034896

Taylor & Francis
Taylor & Francis Group

A multi-sensor approach for mapping plant-derived carbon storage in Amazonian podzols

O.J.R. Pereira[a]*, C.R. Montes[a], Y. Lucas[b], R.C. Santin[a], and A.J. Melfi[c]

[a]*CENA, NUPEGEL, Universidade de São Paulo, Piracicaba, Brazil;* [b]*PROTEE, Université de Toulon, La Garde, France;* [c]*IEE, NUPEGEL, Universidade de São Paulo, Piracicaba, Brazil*

(*Received 13 November 2014; accepted 18 February 2015*)

The Rio Negro basin is characterized by the extensive occurrence of podzol-type soils that store large amounts of organic matter in depth, resulting in the storage of carbon able available to the atmosphere with climate change. The quantification of this carbon requires determination of podzol types and their spatial distribution. Remote-sensing techniques would be helpful in indirect spatializing and segmentation of soil groups in Amazonian podzols. Here we associated remote-sensing images (Shuttle Radar Topographic Mission (SRTM), Operational Land Imager sensor/Landsat 8, and Thermal Infrared Sensor/Landsat 8) and field sample data in order to achieve carbon stock mapping. We found that a multi-sensor approach was critical for a proper segmentation of vegetation groups and spatial distribution of areas with different hydrologic soil regimes.

1. Introduction

The Amazon region is in urgent need of detailed soil mapping covering hitherto relatively undiscovered remote areas, such as those located in the high Rio Negro basin. These areas were mapped between 1970 and 1985 within the framework of the RADAMBRASIL project, the first effort aimed at mapping the whole Brazilian Amazon region, through a combination of aerial Synthetic Aperture Radar (SAR) imagery and scarce soil and rock field controls. The resulting maps were published at a scale of 1:1,000,000 and covered the whole Brazilian Amazon forest area. In 2008, the Brazilian Institute of Geography and Statistics (IBGE) provided a new soil mapping of the Amazon region at a scale of 1:250,000 (IBGE 2008): the RADAMBRASIL data were refined using Landsat imagery and new field data. Although these maps represented a major advance when compared with the RADAMBRASIL maps, they are restricted by a low level of detail, insufficient with regard to requirements related to soil and forest protection and management purposes.

The Rio Negro basin is located in the northwestern part of the central Amazon plain. It mainly consists of an extensive, low-altitude peneplain, some 10–20 m above average river levels (60–90 m above sea level) with scarce relictual inselbergs and mesas. Elementary landscape units are mainly flat plateaux with dispersed and ramified depressions in their centre and, at the edge of the plateaux and in more dissected areas, flat-top to convex hills. Narrow alluvial terraces are observed in major river corridors. Soils in the dissected, better-drained areas are ferralsols and acrisols while the plateaux are occupied by gleyic plinthosols and hydromorphic podzols (BRASIL 1977; Dubroeucq, Volkaff, and

*Corresponding author. Email: ojrpereira@cena.usp.br

Faure 1999; Nascimento et al. 2004). Such soil diversity reflects on the physiognomy and spectral signatures of the vegetation that grades from typical evergreen forest (high rainforest) to forest with a higher density of smaller trees (campinarana) and shrub savannah (campina). Maps from the RADAMBRASIL project (1972–1978) reveal such diversity and the close relationship between vegetation and soil types.

Podzolization in Amazonia has been studied by several authors (Lucas et al. 1984; Dubroeucq and Volkoff 1998; Dubroeucq, Volkaff, and Faure 1999; Nascimento et al. 2004; Montes et al. 2007; Bueno 2009), who have shown its importance as the main process of differentiation of Amazonian ecosystems. Podzols develop with time at the expense of clayey soils, constituting an endmember of soil evolution in such areas. The evolution of the soil systems in the Rio Negro basin is closely connected to the geomorphological pattern of the region. Red and yellow clayey ferralsols and acrisols are found at the edge of dissected low plateaux; by contrast, podzols are found in poorly drained depressions in the central parts of the plateaux. In podzols, the organic matter produced in the topsoil is transferred at depth through sandy eluviated horizons and accumulates at a depth varying from 1 m to more than 10 m, forming thick horizons rich in organic matter, called spodic horizons (Bh). The resultant podzols can store considerable amounts of carbon at depth and thus represent an important carbon pool at the global scale (Montes et al. 2011).

The significant increase in CO_2 emissions over recent decades led in 2005 to the introduction of the programme Reducing Emissions from Deforestation in Developing Countries: Approaches to Stimulate Action (REDD), a mechanism developed under the United Nations framework. This initiative establishes mitigation actions aiming to avoid deforestation in developing countries (UNFCCC 2007; REDD 2014). With the aim of implementing the REDD proposal, recent surveys have been searching for advanced methods and techniques that would allow the detailed spatialization of different types of vegetation cover in order to better understand the distribution of carbon stored in plant biomass and in the first few centimetres of soil (Saatchi et al. 2007).

The complexity of tropical ecosystems, with their high diversity of plant species, decreases the accuracy level of the quantification of carbon stored in vegetation and soil. Therefore, some studies developed over recent decades have been searching for innovative techniques to spatialize carbon with the aid of multi-criterial analysis, which facilitates the correlation between environmental variables that can be inferred by remote-sensing techniques and the concentration of organic carbon stored in vegetation and soil.

Most spatialization methods disregard the occurrence of soil organic carbon (SOC) stored at depths greater than 0.3 m. According to most studies conducted in the Amazon, the carbon stock in soils was estimated around 6–9.4 kg C m^{-2} considering the first 0.3 m of soil (Bernoux et al. 2002), but recent research (Montes et al. 2011) showed that in hydromorphic podzols the carbon stock can exceed 66.7 kg C m^{-2} (0–5 m). Such values suggest that the carbon stored in hydromorphic podzols might represent a significant part of the total organic carbon (TOC) stored in the Amazonian biome. Thus, the carbon stored in thick spodic horizons should not be overlooked in studies that aim to estimate CO_2 emissions in tropical regions while considering the scenario of global climate change.

Taking into account the scarcity of studies that quantify and spatialize the TOC stored in Amazon podzols, the present research aimed to propose association methods between biophysical variables derived from remote-sensing images and field sample data to identify areas of podzols under different hydrologic soil regimes.

2. Methodology

2.1. Study area

The study area was selected after interpretation of spectral vegetation signatures (Landsat/OLI) and with the aid of soil maps (IBGE 2008). It covers an area of 71 km^2 located north of Barcelos City, Amazon State, Brazil, at the central coordinates 0° 15′ 18″ N and 62° 46′ 36″ W (Figure 1). The geological substratum is the sedimentary cover of the rivers Branco and Negro, with some younger depositional areas surrounding the Demeni river (Holocene alluvium of Demeni river; BRASIL 1977). Three soil types developed in the area according to IBGE (2008): ferralsols, gleysols, and podzols.

The light green region on the multispectral composition (Figure 1) indicates the soil association podzol–ferralsol, while the darker green and reddish regions indicate podzols at different stages of evolution (soil drainage conditions). Considering the difficulties involved in accessing the whole study area, a representative zone of soil lateral variability was selected for field investigations and further extrapolation.

2.2. Field data

Ten profiles representative of the three soil units were selected for detailed soil description and sampling. Several other observation points were also selected to determine the occurrence of podzols. Observations and sampling were done by hand-auger drilling. Casing the auger holes with PVC tubes was necessary because of the collapse of the sandy material overlying the spodic horizons when digging or trading. TOC in samples was measured by the dry combustion technique using a Shimadzu TOC-5000 apparatus.

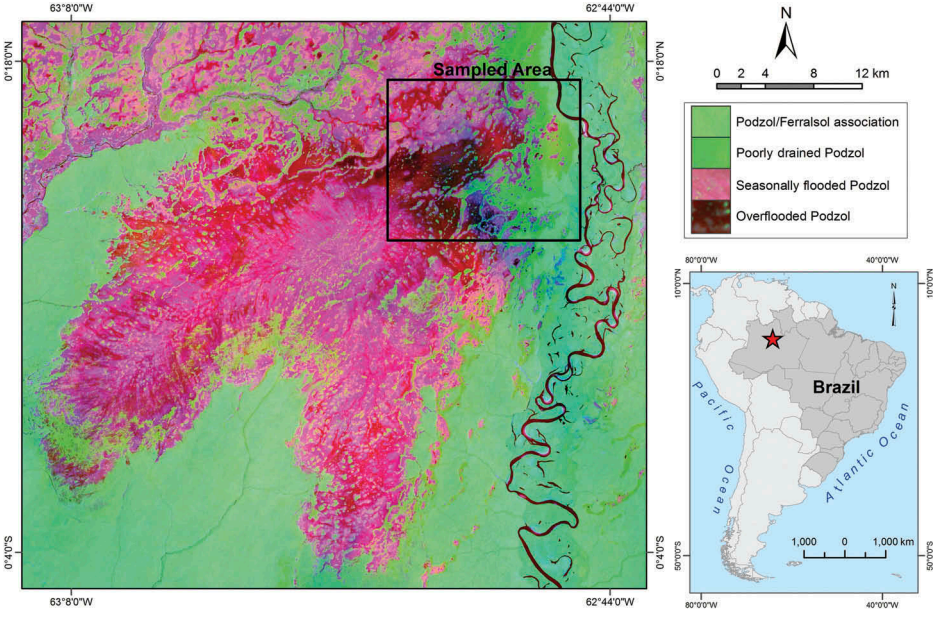

Figure 1. Situation of the study area. The sampled area represents the region where the soil samples were collected. The map illustrates the extrapolation area (multi-sensor composition: Land Surface Temperature, SAVI, and NDMI – R, G, B, respectively).

2.3. Image data and processing methods

Podzol mapping was achieved using remote-sensing images from the Landsat 8 (Operational Land Imager (OLI) and the Thermal Infrared Sensor (TIRS)) and Shuttle Radar Topographic Mission (SRTM) digital elevation models (DEMs), provided by USGS (2014). The Landsat 8 cloud-free composition (path 233, row 60) was acquired on 25 January 2014 at the central coordinates 63° 1′ 55.81″ W; 0° 3′ 33.08″ N. The Landsat bands and the SRTM image were registered by image-to-image registration, to the Landsat 7 ETM+ (Enhanced Thematic Mapper Plus) composition corrected and orthorectified (GLCF 2009). For this composition the positional accuracy on the final image product always has a root mean square error (RMSE) greater than 50 m. Given the foregoing, all the derived products were referenced according to the horizontal accuracy achieved based on the Landsat 7 ETM+ composition systematically corrected and orthorectified. After these procedures, the methods shown in Figure 2 were adopted.

The soil cover in the study area is a mixture of natural vegetated regions and bare soil, mostly white sand zones, with different moisture concentrations. The soil water content, the phytophysiognomy, and the soil type vary according to the topography and hydrologic soil regime. Such aspects can be mapped by remote-sensing images: the products described below were generated from the atmospherically calibrated Landsat/OLI-TIRS bands and SRTM DEM. All derived products were generated taking into account the lateral variation in biophysical properties of soils and vegetation (e.g. topography, surface moisture, surface temperature, and vegetation density).

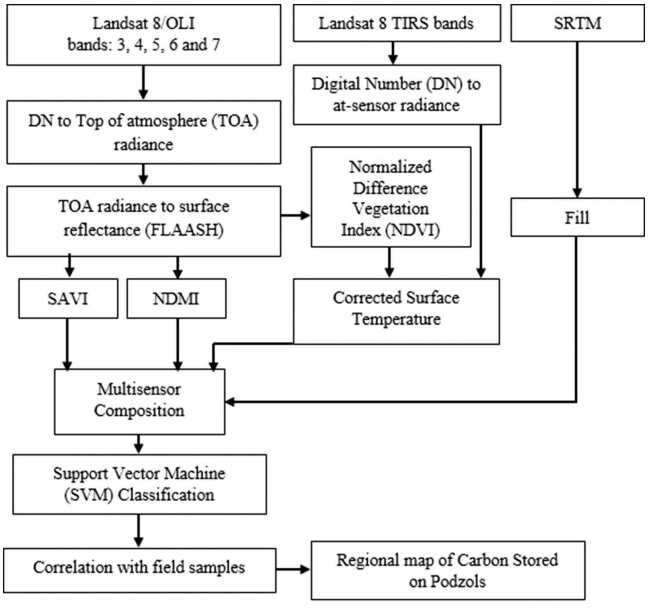

Figure 2. Flow chart showing the methodology employed in this work for generating the regional map of carbon stock. SAVI, soil adjusted vegetation index; NDMI, normalized difference moisture index.

2.3.1. SAVI and NDMI indices

The Landsat OLI bands were atmospherically corrected using the FLAASH Model (ENVI®) in order to derive the surface reflectance. The parameters used in this correction were set to the tropical model. No cloud-masking process was required since the image used was a cloud-free scene. The 5S physically based calibration model MODTRAN (Adler-Golden et al. 1999; Berk et al. 2002) was applied with the aerosol model set to rural, the initial visibility set to 35 km, and an ISAACS multi-scatter model. This method was applied for calibrating the following bands: green, red, NIR, SWIR 1, and SWIR 2 (OLI bands 3, 4, 5, 6, and 7, respectively).

After channel calibration, the SAVI and NDMI (Goodwin et al. 2008) indices were generated from Equations (1) and (2), respectively, the resulting synthetic bands having 30 m spatial resolution and pixel values ranging from −1 to +1:

$$\mathrm{SAVI} = \frac{(1+L) + \left(\mathrm{NIR}_{\rho sur} - R_{\rho sur}\right)}{\left(\mathrm{NIR}_{\rho sur} + R_{\rho sur} + L\right)}, \tag{1}$$

where L (correction factor according to vegetation cover density) is set to 0.5, and $\mathrm{NIR}_{\rho sur}$ and $R_{\rho sur}$ are, respectively, the NIR and Red OLI bands atmospherically corrected.

$$\mathrm{NDMI} = \frac{\mathrm{OLI}\ 5 - \mathrm{OLI}\ 6}{\mathrm{OLI}\ 5 + \mathrm{OLI}\ 6}. \tag{2}$$

This index contrasts the NIR band (OLI 5), which is sensitive to the reflectance of leaf chlorophyll content, to the mid-infrared band (OLI 6), which is sensitive to the absorbance of leaf and soil moisture.

2.3.2. Surface temperature

The thermal bands (TIRS/Landsat 8) 10 and 11 were calibrated to surface temperature as follows. The digital numbers (DNs) of the TIRS bands were converted to the top-of-atmosphere (TOA) radiance from Equation (3):

$$L_{\mathrm{TOA}} = M \times (\mathrm{DN}) + b, \tag{3}$$

where L_{TOA} is the cell value as radiance ($\mathrm{Wm^{-2}\ sr^{-1}\ \mu m^{-1}}$), DN is the digital number, M is the radiance multiplier (0.0003342), and b is the radiance add (0.1). The equation was applied for both thermal raw TIRS bands (10 and 11).

After conversion of DN to TOA, the surface radiance was calculated using the Reference Channel Emissivity (RCE) method. According to this procedure, all the pixels of the thermal channel have a constant emissivity (ε) usually set to 0.95. According to another method described by Sobrino, Jimenez-Munoz, and Paolini (2004), the emissivity may depend on the soil cover. It is thus necessary to consider three different cases: (1) bare ground, (2) fully vegetated, and (3) mixture of bare soil and vegetation. The third case was applied in this study, and hence Equation (4) was used to calculate the emissivity (ε_v):

$$\varepsilon_v = 0.004\ P_v + 0.986, \tag{4}$$

where ε_v is the land surface emissivity (LSE); 0.986 is the standard emissivity value for vegetation and soils; 0.004 is the mean standard deviation value for the emissivity of soils included in the ASTER spectral library (http://asterweb.jpl.nasa.gov) and filtered according to the band TM6 (Landsat 5) filter function (Sobrino, Jimenez-Munoz, and Paolini 2004); and P_v is the vegetation proportion obtained from Equation (5):

$$P_v = \left[\frac{\mathrm{NDVI} - \mathrm{NDVI}_{\min}}{\mathrm{NDVI}_{\max} - \mathrm{NDVI}_{\min}}\right], \tag{5}$$

where NDVI (normalized difference vegetation index), ranging between −1 and +1, is calculated from Equation (6); $\mathrm{NDVI}_{\min}$ is 0.2 and $\mathrm{NDVI}_{\max}$ is 0.5 for a mixture of bare soil and vegetation:

$$\mathrm{NDVI} = \left[\frac{\mathrm{OLI}\ 5 - \mathrm{OLI}\ 4}{\mathrm{OLI}\ 5 + \mathrm{OLI}\ 4}\right], \tag{6}$$

where OLI 4 and OLI 5 correspond to the red and infrared channels of the OLI sensor (Landsat 8), respectively. As indicated by Sobrino, Jimenez-Munoz, and Paolini (2004), a more accurate measurement of NDVI can be obtained by the use of bands atmospherically calibrated.

The final step involves the conversion of the radiance image to spectral emissivity obtained from Equation (3), according to the nature of the surface. For this purpose, the TIRS 10 and 11 radiance bands were converted to TOA temperature by the Equation (7) (NASA 2009):

$$T = \frac{K_2}{\ln\left(\frac{K_1}{L_\lambda} + 1\right)}, \tag{7}$$

where K_1 is the calibration constant 1 (774.89 W m^{-2} ster^{-1} μm, for band 10 and 480.89 W m^{-2} ster^{-1} μm for band 11); K_2 is the calibration constant 2 (1321.08 for band 10 and 1201.14 for band 11); and L_λ is the at-sensor radiance calculated from Equation (3). After this conversion, the surface temperature images were generated from Equation (8) (Weng, Lu, and Schubring 2004):

$$T_s = \frac{T_B}{1 + (\lambda[T_B/\rho])ln_\varepsilon}, \tag{8}$$

where T_B is the blackbody temperature from Equation (7); λ is the wavelength of emitted radiance (band 10: 10.89 μm; band 11: 12.15 μm); ρ is the multiplication of the Boltzmann constant by Planck's constant divided by the velocity of light – 0.01438; and ln_ε is the land surface emissivity (ε_v) calculated from Equation (4). The resulting images from Equation (6) are given in kelvin.

2.3.3. SRTM-filled DEM

The main purpose of this procedure was to create a SRTM DEM free of sinks, which simplifies interpretation of the drainage pattern and the identification of the different

topographic gradients in the study area. It is therefore necessary to identify the sinks and to compare with the DEM to determine whether they have to be eliminated. Given this, a depression-less SRTM DEM was created and the result was used to fill the original DEM.

The study area is a flat zone covered by rainforest with strongly dissected residual hills and poorly drained depressions at the central parts of the podzol plateaux. Because the SRTM DEM was acquired by SAR sensors on the X band, which has a low capacity for penetration in the upper tree canopy, it is sensitive to the texture of the vegetation canopy. Thus, the main purpose of the applied method was to remove the small sinks associated with textural variation in the tree canopies.

The generation of drainage flow direction allowed the estimation of the sinks used to determine the fill limit. After sink identification, their central areas were used to estimate the pour points, allowing the generation of each sink watershed. Untimely, the minimum elevation in each sink watershed was calculated to estimate the average fill limit. The resulting image is a DEM of 30 m spatial resolution (1 arc second data set: SRTM GL1 provided by USGS 2014).

2.3.4. *Image classification and generation of soil maps*

This study attempted to classify the objects into seven regions of interest (ROIs) according to the soil cover associated with the vegetation, surface temperature, surface moisture, and topography: (1) ferralsol–podzol association covered by high, dense rainforest (HRF); (2) poorly drained podzols associated with campinarana forest; (3) depositional zones (alluvial gleysols covered by dense forest and hygrophilous vegetation); (4) incised plains and depressions with seasonally flooded podzols; (5) overflooded podzols covered by herbaceous vegetation; (6) regions of water bodies and permanent flooded areas; and (7) sandbanks and bare soils.

The ROIs were identified in the study area from field observations, regional maps (IBGE 2008), visual interpretation of the spectral signature of the targets (Landsat 8 multispectral composition), and visual interpretation of IKONOS II mosaics in specific zones (where cloud-free scenes were available). The classification of the multi-sensor composition was carried out using the Support Vector Machine (SVM) technique, according to the seven ROIs described above.

A SVM algorithm separated the different ROIs by a hyperplane (Vapnik 1998). The points lying on the boundaries were the support vectors and the middle of the margin was the optimal separating hyperplane. An optimum hyperplane was determined using a training data set (ROI), and its generalization ability was verified using a validation data set (field-truth). The study used a polynomial kernel and employed a 'one-against-one' technique to allow the multi-class classification. The SVM algorithm was implemented in ENVI® software (ITT 2009).

Classified images using the SVM classifier were generated for both multi-sensor composition (NDMI, SAVI, land surface temperature, and filled SRTM) and multispectral OLI composition for statistical comparison. Besides, the SVM classifier was applied for both compositions according to the ISODATA unsupervised classification procedure in order to verify the quality of the multi-sensor composition in comparison to multispectral data of OLI Landsat bands. This procedure does not require human intervention that potentially biases classification and determines the differentiability among spectral classes, giving a better comparison parameter.

Considering that ISODATA is a fully automated method, there is no possibility of interference with the designation of the classes and thus the validation of the classified

images was done by comparison between the automatically generated classes and the field-truth established for the study areas.

2.4. Soil map and correlation with field sample data

For each individual profile, the organic carbon stock was estimated by the following equation:

$$\mathrm{SOC_s} = \sum_{i=1}^{n} B_i C_i D_i, \tag{9}$$

where $\mathrm{SOC_s}$ is the SOC stock (kg C m^{-2}); B_i is the soil bulk density (mg m^{-3}) of layer i; C_i is the proportion of organic carbon (g C g^{-1}) in layer i; and D_i is the thickness (m) of layer i. The average soil density for podzol horizons (D_{bi}) was calculated from surveys previously carried out in the Amazon region by Du Gardin, Grimaldi, and Lucas (2002) and Montes et al. (2011), and directly determined by the Kopeck ring method, with a 70.49 cm^3 cylinder (3.8 cm height and 4.86 cm diameter). The SOC for each soil map unit was then estimated according to its corresponding area in the study site, and then extrapolated at the regional scale.

Soil mapping and segmenting at the regional scale was achieved using products derived from the Landsat sensors and related to the soil cover: biophysical properties of the vegetation and soils (SAVI/NDMI indices), thermal behaviour of the soil surface (temperature images), and surface texture derived from the filled SRTM DEM for segmentation of topographic gradients. The resulting images were applied to estimate the regional behaviour of the biophysical characteristics related to soil type.

3. Results and discussion

3.1. Vegetation and topographic features related to lateral variation in podzols

According to field observations, changes in soil cover occur abruptly in accordance with soil type. Given this, we identified three major soil domains related to podzols.

The first group is dominant in the landscape, and consists of seasonally flooded and overflooded podzols. The vegetation is strongly correlated with the topography, with herbaceous campina in depressed flooded areas and scrubland in adjacent plateaux and, in some regions, patches of bare white sand where grasses and lichens grow according to the seasonality of the region. According to both IBGE (2008) and field observations, bare white sand patches can be considered as gleysols – or podzols with low SOM content in topsoil horizons due to occasional dryness of topsoil material.

The second soil group belongs to the Rio Branco geomorphological domain, with poorly drained podzols. According to IBGE (2008), this area is dominated by tabular hills with vast flat interzones. Field surveys, however, have shown that this domain is a flat landform whose elevation ranges from 50 to 60 m above sea level and covered by campinaranam with scattered HRF patches related to better-drained podzols. Therefore, the phytophysiognomies comprise an ecotone. Ferralsols were not observed in this group.

The third soil group comprises well-drained podzols and ferralsols covered by HRF. This area is characterized by a slight inclination towards the drainage network. Ferralsols may occur punctually in scattered hills 2–10 m above flat, sandy inter-hill surfaces.

The segmentation of the three major groups mentioned above was carried out by a clustering group analysis, considering a Delaunay triangulated relationship between 1000 random samples for the following images: SAVI, relief (SRTM), NDMI, and land surface temperature (arithmetic mean of approximately 186 pixels for each sample). Temperature and SAVI demonstrated an inverse polynomial relationship (Figure 3(*a*)); the correlation between relief and SAVI is better illustrated by a third-order polynomial regression (Figure 3(*b*)) and by a linear relationship for the variables NDMI and SAVI (Figure 3(*c*)).

The inverse correlation between LST and vegetation density (SAVI) indicates that the areas with the highest vegetation indices (HRF from Group 3 and campinarana from Group 2) also have the lower canopy temperatures, which is consistent with their location on hills and tabular tops. Group 2 has a spectral behaviour similar to Group 3, although it may be found in low lands as a sclerophyllous campinarana with slightly higher canopy temperatures. Group 1 has a wide range of temperature, moisture indices, and vegetation

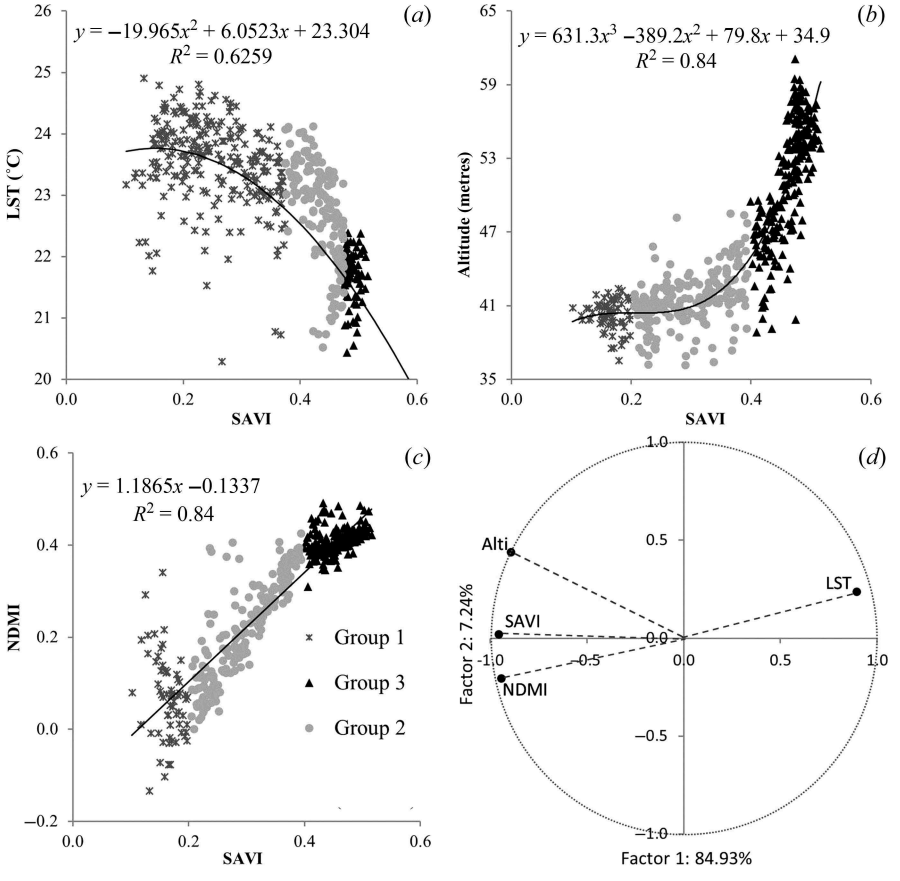

Figure 3. Scatterplot showing the relation between soil adjusted vegetation index (SAVI) and the following variables: (*a*) land surface temperature (LST); (*b*) altitude; and (*c*) normalized difference moisture index (NDMI). (*d*) Projection of the normalized factor coordinates of variables (biophysical variables) in the 1 × 2 factor plane obtained by principal component analysis. Group 1: seasonally flooded and overflooded podzols. Group 2: poorly drained podzols. Group 3: well-drained podzols and ferralsols.

indices, which is consistent with the variety of soil cover and the high temperatures that can occur in herbaceous or bare sand areas under drier conditions.

Taking into account the principal component analysis of the remote-sensing variables, the first principal component (factor 1) accounted for a variance of 84.9% and the second of 7.2%, which corroborates the assumption of a gradual lateral variation in biophysical parameters, from regions of HRF to zones with bare soils and grasses. We observed that this pattern is properly modelled by a general approach involving the study area at the regional scale. However, smaller variations associated with each group must be explained by local models within each cluster group.

According to the distribution of the clusters, Group 1 corresponds to extensive podzols areas located in depressed regions. Both field surveys and remote-sensing images have shown that the surface moisture in such areas can vary laterally according to the topography and vegetation cover (Figure 3(*c*)). The differences in relief were not detectable in the SRTM images considering that the larger height differences are around 1.5–2 m. Such height differences, however, are not negligible in the context of podzol lateral differentiation: the wettest areas allow humic topsoil horizons that are absent in drier areas.

It is important to highlight that lateral variations in the soil mantle in Group 1 are not abrupt like in other areas (Groups 2 and 3). As observed in the field, all intermediaries exist between soils with low SOM content in the topsoil (bare white sand) and those with a high-SOM topsoil horizon (O horizon). This has to be considered for segmentation and to estimate the soil carbon stock in different environments.

3.2. *Classification of soil cover and generation of regional soil map*

The land cover/soil thematic maps were produced from the multi-sensor (OLI/TIRS/SRTM) and OLI multispectral composition according to the SVM classification. The same method, based on ROIs selected for the same known targets (field-truth), was applied to the Landsat OLI multispectral composition (Green, Red, Near Infrared, SWIR 1, and SWIR 2 bands). The ISODATA classifier was applied to both multi-sensor and OLI multispectral compositions (the ISODATA clustering method was used simply for comparison between compositions). The accuracy assessment was then based on the computation of the overall accuracy (OA), producer's accuracy (PA), user's accuracy (UA), and kappa coefficient (Kc) (Congalton and Green 1999), in order to evaluate and compare compositions adopting field surveys as ground truth.

The overall indices of the ISODATA classification were 53.0 % and 63.9% for the OLI multispectral composition and the multi-sensor composition, respectively. Given this, and taking into account an optimized unsupervised classification with identical parameters for both compositions, we observed that the classifications were similar. The multi-sensor composition, however, gave results closer to the reality (ROI) with a better Kc when compared with the OLI composition (0.52 *versus* 0.45), and better PA and UA for most classes (Table 1).

Both compositions were able to segment the three major clustering groups and the variations within each group, but returned high levels of omitted targets for those classes that were correlated to similar targets (Table 1). The unsupervised classification of the OLI multispectral composition has areas of seasonally flooded podzols (Class 4) associated with other targets having closer spectral behaviour, such as regions of overflooded podzol (Class 5) and depositional zones (Class 3). With regard to the multi-sensor composition, we observed a higher level of confusion related to Classes 2 and 3 due to their close

Table 1. Producer's and user's accuracies (PA and UA, respectively) for ISODATA clustering according to the field-truth (ROI). The classes of water bodies and bare soils are not shown.

	Multi-sensor composition		OLI composition	
Class*	PA (%)	UA (%)	PA (%)	UA (%)
Class 1	99.90	47.41	94.11	94.47
Class 2	36.00	90.78	86.50	65.74
Class 3	28.12	16.70	19.54	15.12
Class 4	95.48	86.09	0.06	0.10
Class 5	90.09	95.23	73.03	95.14

Note: *Class 1: Ferralsol–podzol association covered by high dense rainforest (HRF). Class 2: poorly drained podzols associated with campinarana forest. Class 3: depositional zones (alluvial gleysols covered by dense forest and hygrophilous vegetation). Class 4: incised plains and depressions with seasonally flooded podzols. Class 5: overflooded podzols covered by herbaceous vegetation.

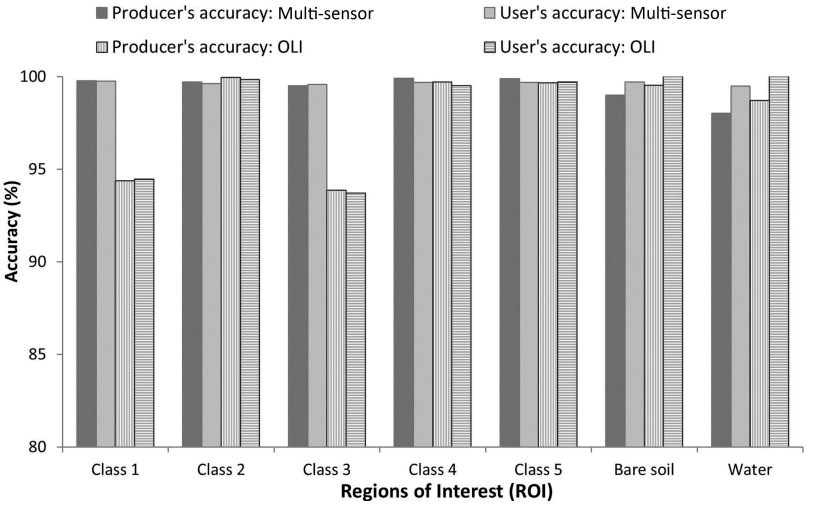

Figure 4. Producer's and user's accuracies for the SVM classification of multi-sensor and OLI Landsat 8 compositions. The designation of each class is shown in Table 1.

spectral similarity. ISODATA clustering was helpful in an unbiased comparison between the two compositions. However, better results were achieved through the application of supervised classification algorithms (Figure 4).

All of the classes in Figure 4 have a PA above 98% for the multi-sensor composition. Such values were achieved according to ground truth observed in field surveys and regional soil maps (IBGE 2008) and thus the classifications might be biased, which must be considered in final maps of soil carbon stock. It is important to highlight the enhanced efficiency of the multi-sensor composition when compared with the OLI multi-spectral composition using the same ROI for both images (Figure 4).

To access an optimum SVM classification algorithm, a range of kernel types, penalty parameters, pyramid levels, and classification probability thresholds was tested until reaching the value closest to the ground truth (Shafri and Ramle 2009). The best result was obtained through a radial basis kernel with a penalty parameter of 100, a pyramid level of 2, and a probability threshold of 0. The OA of such classification was 99.65%

Table 2. Confusion matrix of the multi-sensor classified image, representing class similarity.

		Ground truth ROI (%)						
	Class*	Class 1	Class 2	Class 3	Class 4	Class 5	Class 6	Class 7
Classified (SVM)	Class 1	99.8	0.0	0.3	0.0	0.0	0.0	0.0
	Class 2		99.7	0.3	0.0	0.0	0.0	0.1
	Class 3			99.5	0.0	0.0	0.0	0.0
	Class 4				99.0	0.0	1.0	0.0
	Class 5					98.0	0.0	1.0
	Class 6						99.0	0.0
	Class 7							99.0

Note: *Class 1: Ferralsol–podzol association covered by HRF. Class 2: poorly drained podzols associated with campinarana forest. Class 3: depositional zones (alluvial gleysols covered by dense forest and hygrophilous vegetation). Class 4: incised plains and depressions with seasonally flooded podzols. Class 5: overflooded podzols covered by herbaceous vegetation. Class 6: bare soils. Class 7: water.

with a Kc of 0.99. For the SVM classification of the OLI multispectral composition, obtained OA and Kc were 96.87% and 0.96, respectively.

The SVM algorithm returned refined results when compared with the ground truth (Table 2), with all classes having a similarity above 98%. However, the ground truth data may be biased due to difficulty in processing detailed field surveys and the low spatial scale of the reference soil map (1:250,000). A detailed visual inspection over the classified image was thus carried out to verify errors and occurrences of incorrect classification. Errors were corrected by changing the pixel values of the original GRID. The regional soil map was then elaborated on the basis of the classified image, with a nominal spatial resolution of 30 m.

3.3. Mapping the depth of carbon stock in podzol regions

Our studies have shown that topsoil and deep SOM-rich podzol horizons can vary laterally in both thickness and carbon content, which means that the carbon stored in podzols is sensitive to local environmental variables such as soil moisture, topography, hydrological regime, geologic substratum, and vegetation cover, as well as regional variables such as temperature and rainfall. The most refined maps available for this region (IBGE 2008) do not consider local variables as relevant factors in regard to the lateral distribution of podzols. The local environmental variables are considered hereafter to allow correlation between soil carbon stocks and biophysical features.

The lateral and vertical variation in carbon content in podzol profiles is related to the relief and the hydrological regime of the region. The first area we investigated was designated as a HRF over podzols and ferralsols. Detailed study of a range of profiles gave a good approximation of the average carbon stock in this domain (Figures 5 and 6). The better-drained areas (HRF over low-hill ferralsols and well-drained podzols) have a large amount of carbon in the first few centimetres of soil (O and A horizons). Deep Bh (depth 1.5–4.5 m) was observed but with a low content of organic carbon (Figure 5). At the transition between this area and the poorly drained podzol region, the deep SOM-rich layers increase and show a higher content of carbon. The third main area comprises extensive regions of overflooded podzols where the presence of Bh was observed.

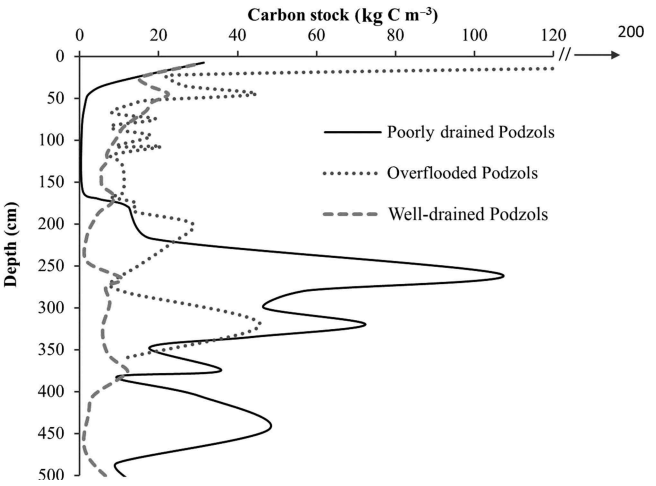

Figure 5. Average carbon stock for the three main podzol groups described in the study area.

The final group consists of herbaceous and flooded areas. The presence of podzols in such areas was disregarded in previous studies (Batjes and Dijkshoorn 1999; Bernoux et al. 2002; Cerri et al. 2007; Saatchi et al. 2007). The topsoil horizons comprise high SOM content. Podzols with bare topsoil store some carbon in their deep Bh, although in smaller quantities than more vegetated podzols, probably because of low production in the topsoil horizons of humic substances likely to accumulate in deep Bh. The high level of moisture in such areas allows the accumulation of a considerable amount of SOC in the topsoil. In this domain we observed that topsoil (first 5 cm) may store more than 200 t C ha^{-1} (Figure 5).

From vegetated podzol areas to bare soil, the amount of carbon stored decreases gradually, until the zones of open sandy fields. According to Stropp et al. (2011), white sand fields have a sparse distribution over the region of the Rio Negro Basin. In the study area, however, these zones follow an insular pattern with highly weathered bare soils in the depressed centre surrounded by SOC-rich podzols on flat areas, then ferralsols at the slightly incised, low-hill borders. Similar patterns were previously observed in other podzol areas (Boulet et al. 1997; Nascimento et al. 2004; Montes et al. 2007, 2011). These authors pointed out that the lateral organization of the ferralsol–podzol soil system indicates its stage of evolution, which is important in estimating carbon stock.

The average carbon stock for each soil group was estimated taking into account the clustering analysis and the soil map derived from the multi-sensor image composition (Figure 6). The greatest amount of carbon stored in depth horizons was found in the poorly drained podzol areas, the lowest in podzols–ferralsols, and intermediate amounts in flooded podzols (Table 3).

The areas of alluvial gleysols and ferralsols have a small amount of carbon stored in horizons deeper than 0.50 m, mostly located in the first few centimetres in the organic layer according to our investigations and values provided by IBGE (2008) for soil samples collected in areas of ferralsols and alluvial gleysols (0–0.5 m: 70.9 ± 27 t C ha^{-1} for ferralsols and 89.9 ± 35.4 t C ha^{-1} for gleysols; below 0.5 m: 31.5 ± 10.7 t C ha^{-1} for ferralsols and 25.8 ± 8.5 t C ha^{-1} for gleysols). In flooded podzols we observed a large amount of carbon stored as poorly decomposed organic matter on the surface (Table 3), due the low microbial activity in this domain. These zones are strongly related to wetlands covered by grasses and

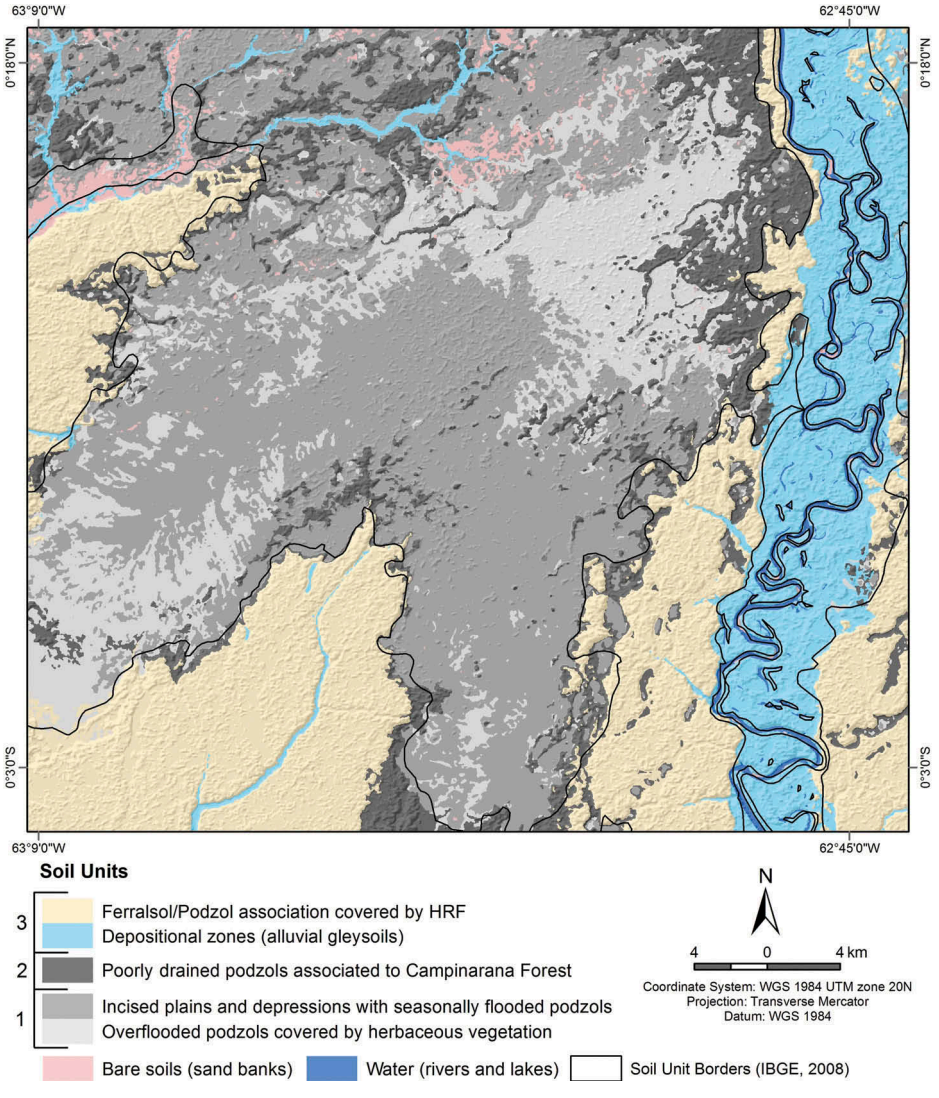

Figure 6. Soil map illustrating the spatial distribution of the soil types. The numbers for the soil units represent the cluster groups described in Figure 3.

Table 3. Average carbon stock in podzols.

Soil group	0–0.50 m Carbon (t ha^{-1})	0.50–4 m Carbon (t ha^{-1})
Poorly drained podzols*	62.80 ± 10.03	477.75 ± 63.9
Flooded podzols†	249.12 ± 18.83	161.22 ± 45.35
Podzol–ferralsol association	84.35 ± 12.4	188.77 ± 38.5

Note: *The average thickness observed for surface and depth horizons was considered according to soil type.
†This class comprises seasonally flooded podzols and overflooded podzols.

Table 4. Total carbon stock, by soil unit. The stock is represented in teragrammes (Tg; 10^{12} g) and the area in hectares (ha).

Class*	C stock (Tg)	Area (ha)	Area (%)†	C stock (%)
Class 1	17.9 ± 6.4	6.47 10^4	26.8	21.7
Class 2	16.1 ± 2.5	3.07 10^4	12.8	19.6
Class 3	4.0 ± 0.4	2.81 10^4	11.7	5.0
Class 4	21.8 ± 5.7	7.88 10^4	32.7	26.5
Class 5	9.7 ± 0.7	3.19 10^4	13.2	11.8
Class 6	–	3.70 10^3	1.6	–
Class 7	–	3.17 10^3	1.3	–

Note: *The designation of each class is shown in Table 2. †The percentage values indicate the range of each unit relative to the total area and carbon stock.

scrubs. Finally, we did not identify a significant amount of carbon stored in areas of bare soil. The range of the soil units and their carbon stock are shown in Table 4.

Previous carbon stock maps for these regions (Bernoux et al. 2002) estimated that podzol areas store about 275 t C ha^{-1} (0–1 m soil thickness), which is lower than our estimation of 415 t C ha^{-1} as average carbon stock in the podzol areas (0–4 m soil thickness) when we take into account the deep SOM-rich podzol horizons.

The most detailed map available for this area (IBGE 2008) shows generalized classes of podzols, ferralsols, and alluvial gleysols (IBGE limits are also reported in Figure 6). The subunits within each soil unit are not designated due to the low level of detail in the soil map. The definition of soil units, according to surveys carried out in previous studies (IBGE 2008), was based on a small number of soil samples. Extrapolation was performed by interpretation of topography (SAR) and the spectral behaviour of vegetation (passive remote-sensing systems). The lack of soil samples and the absence of detailed biophysical data are the main reasons for the misclassification of some soil units. As an example, some ferralsol–podzol associations mapped on Figure 6 were defined by IBGE (2008) as ferralsols. According to our observations, ferralsols in these areas occur as scattered, well-drained hills that can only be mapped at a local scale.

Taking into account the carbon soil contents defined in this study and using the IBGE (2008) soil delimitation, the calculation of soil carbon stored in the study area yields 0.65 Pg when using the IBGE (2008) soil delimitations and 0.81 Pg when using the soil map derived from the multi-sensor image composition. Such a discrepancy highlights the need for mapping the high Rio Negro basin at a regional scale, allowing for a more accurate estimation of the carbon stored in soils. The correct estimation of SOC stock at a regional scale in such a complex environment depends on both the availability of soil samples suitable to represent both the lateral and vertical variability of the soil units and the association with biophysical parameters inferred by remote-sensing data.

4. Conclusions

A multi-sensor approach proved crucial to mapping the soil carbon stock at the regional scale in regions of hydromorphic soils in the high Rio Negro basin characterized by wide lateral and vertical variability in carbon stock. The quantity of carbon stored in soils is related to environmental aspects such as topography, vegetation type, and soil surface moisture, which can be indirectly inferred by remote-sensing images through a range of data sets collected by various sensor systems and orbital satellite platforms. The

combination of these data sets allowed a better understanding of the aspects related to soil variability, when combined with field sample data.

According to our study, podzols from depressed overflooded and poorly drained areas of sclerophyllic vegetation store considerable amounts of carbon in deep horizons that can range from 2 m to more than 10 m. Pre-existing maps have only a low level of detail, and field-truth was based on scarce soil observations. Moreover, the soil profiles used in previous field surveys are limited to depths of no more than 1 m, which is inadequate to investigate the level of SOC stored in podzol Bh horizons.

Disclosure statement

No potential conflict of interest was reported by the authors.

Funding

This work was funded by grants from Brazilian FAPESP (São Paulo Research Foundation) and CNPq, and French ARCUS (joint programme of Région PACA and French Ministry of Foreign Affairs).

References

Adler-Golden, S. M., M. W. Matthew, L. S. Bernstein, R. Y. Levine, A. Berk, S. C. Richtsmeier, P. K. Acharya, G. P. Anderson, J. W. Felde, J. A. Gardner, M. L. Hoke, L. S. Jeong, B. Pukall, A. J. Ratkowski and H. K. Burke. 1999. "Atmospheric Correction for Short-wave Spectral Imagery Based on MODTRAN4." *SPIE Proceeding* 3755: 1–10. doi:10.1117/12.366315.

Batjes, N. H., and J. A. Dijkshoorn. 1999. "Carbon and Nitrogen Stocks in the Soils of the Amazon Region." *Geoderma* 89: 273–286. doi:10.1016/S0016-7061(98)00086-X.

Berk, A., L. S. Bernstein, G. P. Anderson, P. K. Acharya, D. C. Robertson, J. H. Chetwynd, and S. M. Adler-Golden. 2002. "Exploiting MODTRAN Radiation Transport Atmospheric Correction: The FLAASH Algorithm." *SPIE Proceeding* 2: 798–803. doi:10.1109/ICIF.2002.1020888.

Bernoux, M., M. D. S. Carvalho, B. Volkoff, and C. C. Cerri. 2002. "Brazil's Soil Carbon Stocks." *Soil Science Society of America Journal* 66: 888–896. doi:10.2136/sssaj2002.8880.

Boulet, R., A. Chauvel, F. X. Humbel, and Y. Lucas. 1982. "Analyse structurale et cartographie en pédologie: I – Prise en compte de l'organisation bidimensionnelle de la couverture pédologique: les études de toposéquences et leurs principaux apports à la connaissance des sols." *Cahiers ORSTOM, Série Pédologie* 19: 309–321.

Boulet, R., Y. Lucas, E. Fritsch, and H. Paquet. 1997. "Geochemical Processes in Tropical Landscapes: Role of the Soil Covers." In *Soils and Sediments – Mineralogy and Geochemistry*, edited by H. Paquet and N. Clauer, 67–96. Heidelberg: Springer-Verlag.

BRASIL. 1977. Ministério das Minas e Energia. RADAMBRASIL Project: Volume SA.19, Theme: Pedologia. Rio de Janeiro, 181–237. (Levantamento dos Recursos Naturais, 14).

Bueno, G. T. 2009. "Appauvrissement et podzolisation des latérites du bassin du Rio Negro et genèse des Podzols dans le haut bassin amazonien." Ph.D. thesis, Institut de Physique du Globe de Paris (IPGP), Instituto de Geografia, Universidade Estadual Paulista "Júlio de Mesquita Filho" (UNESP), Paris, 193 pp.

Cerri, C. E. P., M. Easter, K. Paustian, K. Killian, K. Coleman, M. Bernoux, P. Falloon, D. S. Powlson, N. H. Batjes, E. Milne, and C. C. Cerri. 2007. "Predicted Soil Organic Carbon Stocks and Changes in the Brazilian Amazon between 2000 and 2030." *Agriculture, Ecosystems & Environment* 122: 58–72. doi:10.1016/j.agee.2007.01.008.

Congalton, R. G., and K. Green. 1999. *Assessing the Accuracy of Remotely Sensed Data: Principles and Practices*, 183 pp. Boca Raton, FL: Lewis.

Du Gardin, B., M. Grimaldi, and Y. Lucas. 2002. "Effets de la déshydratation sur les sols du système ferralsol-podzols d'Amazonie centrale. Reconstitution de la courbe de désorption d'eau à partir de la porosimétrie au mercure." *Bulletin de la Societe Géologique de France* 173: 19–34.

Dubroeucq, D., B. Volkaff, and P. Faure. 1999. “Les couvertures pédologiques à podzols du bassin du haut Rio Negro (Amazonie).” *Etude et gestion des sols* 6: 131–153.
Dubroeucq, D., and B. Volkoff. 1998. “From Oxisols to Spodosols and Histosols: Evolution of the Soil Mantles in the Rio Negro Basin (Amazonia).” *Catena* 32: 245–280. doi:10.1016/S0341-8162(98)00045-9.
Global Land Cover Facility (GLCF). 2009. “Landsat GeoCover.” Maryland. Accessed May 4, 2014. http://glcf.umiacs.umd.edu/data/landsat/
Goodwin, N. R., N. C. Coops, M. A. Wulder, S. Gillanders, T. A. Schroeder, and T. Nelson. 2008. “Estimation of Insect Infestation Dynamics Using a Temporal Sequence of Landsat Data.” *Remote Sensing of Environment* 112: 3680–3689. doi:10.1016/j.rse.2008.05.005.
IBGE. Geoscience Department (DGC). 2008. “Coordenação de Recursos Naturais e Estudos Ambientais (CREN).” Mapas georreferencias de recursos naturais. Scale 1:250:000, Digital Format: shp. Rio de Janeiro. Accessed August 15, 2014. ftp://geoftp.ibge.gov.br/mapas/
ITT. 2009. “Visual Information Solutions.” Accessed January 20, 2014. http://www.envi.com.br/index.php?link= Atmospheric_Correction.
Lucas, Y., A. Chauvel, R. Boulet, G. Ranzani, and F. Scatolini. 1984. “Transicão latossolos-podzois sobre a formação Barreiras na região de Manaus, Amazônia.” *The Revista Brasileira de Ciencia do Solo* 8: 325–335.
Montes, C. R., Y. Lucas, A. J. Melfi, and D. A. Ishida. 2007. “Systèmes sols ferrallitiques–podzols et genèse des kaolins.” *Comptes Rendus Geoscience* 339: 50–56. doi:10.1016/j.crte.2006.11.001.
Montes, C. R., Y. Lucas, O. J. R. Pereira, R. Achard, M. Grimaldi, and A. J. Melfi. 2011. “Deep Plant-Derived Carbon Storage in Amazonian Podzols.” *Biogeosciences* 8: 113–120. doi:10.5194/bg-8-113-2011.
NASA. 2009. “Landsat 7 Science Data Users Handbook.” Maryland. Accessed January 15, 2014. http://landsathandbook.gsfc.nasa.gov/pdfs/Landsat7_Handbook.pdf
Nascimento, N. R., G. T. Bueno, E. Fritsch, A. J. Herbillon, T. Allard, A. Melfi, R. Astolfo, H. Boucher, and Y. Li. 2004. “Podzolization as a Deferralitization Process: A Study of an Acrisol-Podzol Sequence Derived from Palaeozoic Sandstones in the Northern Upper Amazon Basin.” *European Journal of Soil Science* 55: 523–538. doi:10.1111/j.1365-2389.2004.00616.x.
REDD. 2014. “Information Sharing Web Platform.” Accessed January 15, 2014. http://unfccc.int/methods_science/redd/items/4531.php
Saatchi, S. S., R. A. Houghton, R. C. Dos Santos Alvalá, J. V. Soares, and Y. Yu. 2007. “Distribution of Aboveground Live Biomass in the Amazon Basin.” *Global Change Biology* 13: 816–837. doi:10.1111/j.1365-2486.2007.01323.x.
Shafri, H. Z. M., and F. S. H. Ramle. 2009. “A Comparison of Support Vector Machine and Decision Tree Classifications Using Satellite Data of Langkawi Island.” *Information Technology Journal* 8: 64–70. doi:10.3923/itj.2009.64.70.
Sobrino, J. A., J. C. Jimenez-Munoz, and L. Paolini. 2004. “Land Surface Temperature Retrieval from LANDSAT TM 5.” *Remote Sensing of Environment* 90: 434–440. doi:10.1016/j.rse.2004.02.003.
Stropp, J., P. Van Der Sleen, P. A. Assunção, A. L. Silva, and H. T. Ter Steege. 2011. “Tree Communities of White-Sand and Terra-Firme Forests of the Upper Rio Negro.” *Acta Amaz* 41: 521–544. doi:10.1590/s0044-59672011000400010.
UNFCCC. 2007. “Reducing Emissions from Deforestation in Developing Countries: Approaches to Stimulate Action.” FCCC/SBSTA/2007/L.23/Add.1/Rev.1. Accessed March 8, 2014. http://unfccc.int/resource/docs/2007/sbsta/eng/l23a01r01.pdf2007
USGS. 2014. “Earth Resources Observation and Science (EROS) Center.” Reston, VA. Accessed September 11. http://eros.usgs.gov/
Vapnik, V. 1998. *Statistical Learning Theory.* New York: John Wiley and Sons.
Weng, Q., D. Lu, and J. Schubring. 2004. “Estimation of Land Surface Temperature–Vegetation Abundance Relationship for Urban Heat Island Studies.” *Remote Sensing of Environment* 89: 467–483. doi:10.1016/j.rse.2003.11.005.